Modeling Radiation Transport Using MCNP6 and Abaqus/CAE

Chelsea A. D'Angelo, Steven S. McCready, Karen C. Kelley
Los Alamos National Laboratory

Abstract: Los Alamos National Laboratory (LANL) has released a new version of MCNP, its general purpose Monte Carlo N-particle transport code, which has the ability to use unstructured meshes created with Abaqus/CAE as geometry descriptions. This improvement allows mechanical engineering models to be used in place of legacy constructive solid geometry descriptions, which are far less sophisticated. This capability also allows for the seamless integration of radiation transport calculations with analysis of the resulting thermal and mechanical effects on materials. Using Abaqus/CAE for visualization of the results calculated by MCNP6 is a major advantage over the previous ability to view results in two-dimensional space with MCNP's native plotter. This presentation will show simple examples drawn from research performed at LANL in order to demonstrate the integration of Abaqus/CAE with MCNP. The example problems will include shielding and criticality applications.

Keywords: MCNP, Radiation Transport, Constructive Solid Geometry, Unstructured Mesh, Shielding, Criticality

1. Introduction

Los Alamos National Laboratory (LANL) has released MCNP6, a new version of its general purpose Monte Carlo N-Particle transport code, which allows the use of unstructured mesh geometry descriptions generated by Abaqus/CAE alongside its legacy constructive solid geometry (CSG) description. The results from the MCNP6 run can then be imported back into Abaqus/CAE for visualization and analysis. This new capability provides an easier and more accurate way of building complex geometries which is a large advantage over CSG. The three dimensional visualization of both the geometry and results is a major improvement over the MCNP plotter that shows two dimensional views of the problem. The MCNP users that currently use CSG descriptions would benefit from having a suite of example models available that compares legacy and new approaches. Also, the code development effort needs to show that results are consistent when comparing calculations that use unstructured mesh geometries to those that use CSG.

A few different types of examples will be available in the manual, and several of those will be presented in this paper. All examples will compare the results from using the legacy CSG and the unstructured mesh as geometry descriptions. The first example will show the attenuation of a monoenergetic photon source passing through a planar sheet of material. A simple, one-dimensional hand calculation will also be compared to the CSG and unstructured mesh MCNP6 runs. Another example is a representation of a gamma irradiation experimental setup at LANL's Ion Beam Materials Laboratory (IBML). The next example is a mock scenario of a steel bar contaminated with cobalt-60 in a room with a lead wall shield. The final example involves an experiment package that was irradiated in Sandia National Laboratory's Annular Core Research Reactor (ACRR). It will show how the Abaqus/CAE unstructured mesh can be embedded within a complex CSG description.

2. Background

MCNP is a general-purpose Monte Carlo N-Particle code that is widely used for neutron, photon, charged particle, and heavy ion transport simulations. The code is used for various applications including radiation shielding, medical physics, nuclear criticality safety, accelerator target design, and fission and fusion reactor design. The MCNP input file contains information about the problem including the geometry specification, description of materials, the location and characteristics of the source, the type of answers desired (flux, dose, energy deposition, etc.), and any techniques used to increase efficiency (X-5 Monte Carlo Team, 2003). The legacy geometry capability of MCNP has proven to work very well for simple configurations that can be easily defined by one and two-dimensional surfaces, but it is limited when it comes to constructing more complex geometries. The process is difficult, time-consuming, and error-prone (Kelley, 2009). For these reasons, code developers chose to implement a hybrid geometry capability into the code that allows users to embed an Abaqus/CAE-generated mesh universe into the legacy constructive solid geometry.

The first step in creating the unstructured mesh geometry description is building solid parts in Abaqus/CAE. The solid parts are then meshed according to the type and size of element desired for the specific application. The elements that make up each part are then grouped into element

sets, or ‘elsets’, so that certain properties, such as a material, can be assigned. These elsets define the pseudo-cells that are part of the cell card section of the MCNP6 input file. The assembly is created by instancing the parts.

Figure 1 below shows a few sections from an MCNP6 input file that uses Abaqus/CAE-generated unstructured mesh as a geometry description. There are two pseudo-cells (lead wall and sphere of air) that are defined with a zero surface and assigned to a universe (Universe 1). The background cell also has surface zero and an assignment to Universe 1. In the surface card section, a spherical surface is described that surrounds the entire mesh geometry. The fill cell (Cell 40) is the area within that spherical surface (Surface 99) and the universe cell (Cell 50) encompasses everything outside of that surface. There is further discussion about the hybrid geometry following the input file. The embed card section contains the rest of the information necessary for communication between the MCNP6 input file and the input file generated by Abaqus/CAE.

```
c CELL CARDS
c Cell | Mat'l # | Density | Surface | Universe
10        82      -11.35       0        u=1     $Lead wall (pseudo-cell)
20        20      -1.205E-3    0        u=1     $Surrounding air (pseudo-cell)
30        20      -1.205E-3    0        u=1     $Background Cell
40         0                  -99     fill=1     $Fill Cell
50         0                   99                $Universe Cell

C SURFACE CARDS
99  S   50 50 0   200                    $Sphere surr. entire mesh geometry

C ABAQUS/CAE EMBEDDED MESH SECTION
embed1    meshgeo=abaqus
          mgeoin=leadwall_abq.inp        $Input file generated by Abaqus/CAE
          meeout=leadwall_abq.eeout      $Name of MCNP6 elemental output file
          filetype=ascii
          background=30                  $MCNP6 background cell
          matcell= 1 10                  $1st part instance (lead wall)
                   2 20                  $2nd part instance (air sphere)
embee4:p embed=1                         $Elemental tally
```

Figure 1. Sections of an MCNP6 input file that uses an Abaqus/CAE unstructured mesh geometry description.

A simple representation of the hybrid geometry is shown in Figure 2. The MCNP6 mesh universe is infinite in extent and contains the Abaqus/CAE unstructured mesh. The fill cell crops the boundaries of the mesh universe. The Abaqus/CAE unstructured mesh must be completely contained within the fill cell boundary. The background cell surrounds the Abaqus/CAE unstructured mesh inside the fill cell and covers any gaps within the mesh. This is important so that transport can still occur if there are gaps in the mesh (Martz, 2011).

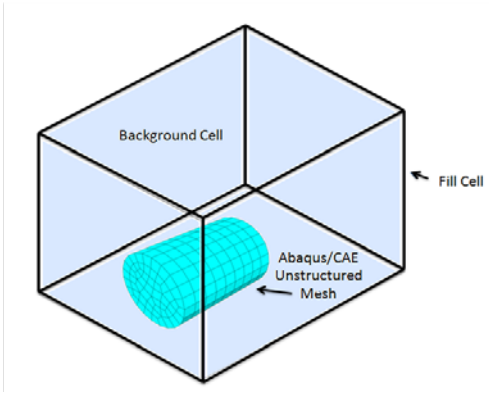

Figure 2. Representation of MCNP mesh universe.

In addition to the ease of use that Abaqus/CAE provides in the creation of the geometry, Abaqus/CAE is also used for three-dimensional visualization of the results from the MCNP6 run. This ability to visualize the results in three dimensions and look at singular parts and elements is a vast improvement over the previously used two-dimensional MCNP plotter. The MCNP6 results that are calculated on the mesh are printed to a separate output file. This output file is converted to a .odb file that can be used by Abaqus/CAE for visualization or as a source term for FEA.

In previous work, the capability of MCNP6 to use Abaqus/CAE unstructured mesh as a geometry description was tested with the well-understood Godiva criticality benchmark (Kelley, 2009). Godiva is an unshielded, pulsed nuclear reactor that was originally located at Los Alamos National Laboratory (Criticality Benchmarks, 2009). It is a simple, highly-enriched uranium sphere of radius 8.74 cm. In criticality calculations, accurate volumes and masses are crucial. This presents a challenge because of Godiva sphere's curved surface which is more difficult to describe with a faceted mesh than with CSG. The Godiva sphere was modeled with different sizes of first and second order hexahedral and tetrahedral elements. Figure 3 shows the total energy deposition results for the Godiva sphere that was meshed with first order tetrahedral elements and a 1.75 cm mesh seed.

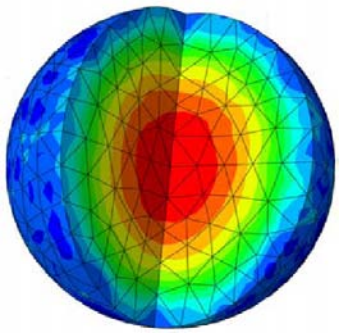

Figure 3. Abaqus/CAE visualization of energy deposition calculated by MCNP6 on the Godiva sphere meshed with first order tetrahedral elements and a 1.75 cm mesh seed.

The results were compared against CSG runs and actual experimental data and can be seen in the report on unstructured meshes for criticality calculations (Kelley, 2009). When the element size is small, the volumes and masses were more accurately reproduced, so good agreement was found. The mesh created with second order elements performed better than those created with first order elements because of the second order elements' ability to possess curvature. In cases where the same number of second order tetrahedral elements and hexahedral elements represent the volume equally well, the calculation with the second order tetrahedral elements will run faster. The convergence of k-effective is faster for second order elements than for first order elements for the same number of elements (Kelley, 2009).

3. Example Cases

The present work builds upon the Godiva example problem. Currently, more complex geometries and different features of the code are being tested. This section will outline each example problem; it will describe the geometry, type of mesh elements, source, and results of each system that was modeled.

3.1 Attenuation of Monoenergetic Photon Source through Material

Lead is a common material used for photon shielding because of its high density and atomic number. Patients at the dentist office wear lead aprons that shield them from x-rays (a type of photon) and lead bricks are used to make walls in radiation facilities to shield workers from gamma rays (another type of photon). To demonstrate the effectiveness of lead as a photon shield, a simple hand calculation was performed along with two MCNP6 calculations, one using CSG and another using Abaqus/CAE geometry. The source is a plane wave of 1 MeV photons directed in a straight line through the thickness of the sheet. The lead sheet is 1 cm thick.

For the hand calculation, the following attenuation equation, Equation 1, was used:

$$\Phi = \Phi_0 * e^{-\Sigma x} \tag{1}$$

where Φ_0 is the incident photon flux in photons/s-cm^2, Φ is the photon flux at a distance x in cm, and Σ is the macroscopic cross section. The macroscopic cross section (the inverse of the average distance the photon will travel before it interacts) describes to what extent the photons will interact with the lead atoms. The same cross section for 1 MeV photons in lead that was used in the MCNP6 calculations was used here. This equation is most accurate if the only result of interaction is absorption. This is a simplification because there are many types of interactions that can occur.

For both the CSG and Abaqus/CAE geometry descriptions, a 1 m x 1 m x 1cm sheet of lead surrounded by a sphere of air was built. The MCNP6 input files contained tallies for total photon flux and number of photons crossing the front and back surfaces of the sheet. The Abaqus/CAE model was meshed with first order hexahedrons.

The following plot, Figure 4, shows a comparison between the simple hand calculation, and the MCNP6 runs using both CSG and Abaqus/CAE unstructured mesh (UM) geometry. The hand calculation only takes 1 MeV photons into consideration while MCNP6 calculations also track photons of lower energies that occur when the 1 MeV photons come in contact with lead atoms. There is near perfect agreement when comparing the hand calculation to the MCNP6 calculations

where only photons of energies greater than 995 keV were considered. However, when considering photons of all energies, a higher flux is calculated.

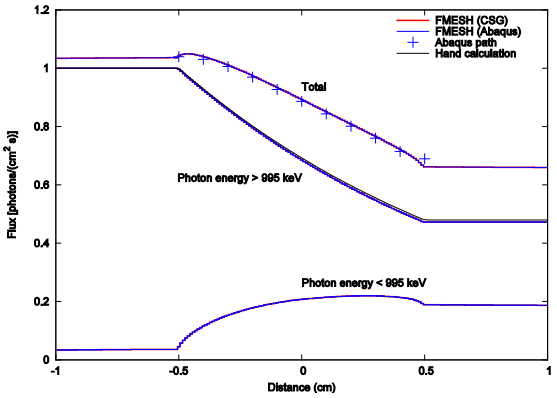

Figure 4. Comparison of photon attenuation calculations. The lead sheet extends from 0 to 1 cm in the plot.

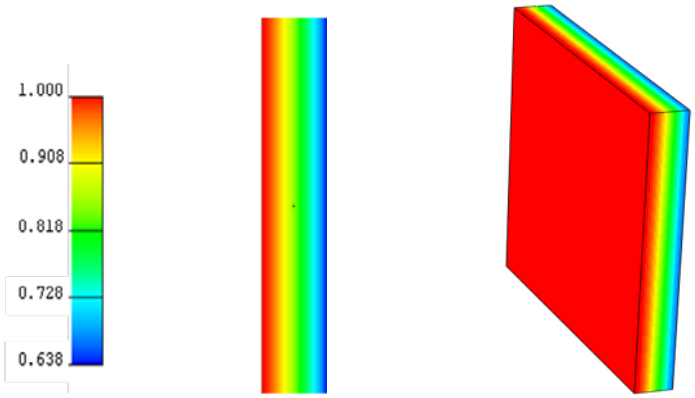

Figure 5. Comparison of visualization of results using MCNP's plotter and Abaqus/CAE. The same scale with units in photons/cm^2-sec, is used for both cases; MCNP6 run using CSG (left) and the run using Abaqus/CAE mesh (right).

Figure 5 shows a comparison in the visualization of photon attenuation through the 1 cm thick lead sheet. Considering the very close agreement seen in the plot above, Figure 3, the results from the visualization appear to be just as close. Even though this particular problem has a simple geometry, the benefit of the three-dimensional visualization can already be seen. Visualization in Abaqus/CAE allows the user to easily manipulate the geometry (rotate, zoom in and out, remove layers, etc.) and also view each part separately.

3.2 IBML Experiment: Gamma Irradiation of Material Sample

The Ion Beam Materials Laboratory at LANL has a 3 MV tandem accelerator and a 200 kV ion implanter along with several beam lines. Attached to each line is a series of experimental stations

that support various research programs (IBML, 2006). One particular experiment is aimed at characterizing gamma irradiation in different materials. The material sample is contained within an aluminum can that is attached to the beam line. The proton beam irradiates a metal target located 0.66 cm away from the bottom of the aluminum can holding the material sample. This produces a flux of 1.6e8 gammas/steradian with an energy of 55 keV. A simple illustration of the setup is shown in Figure 6.

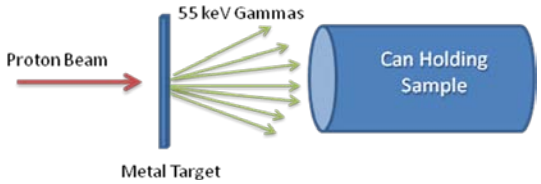

Figure 6. Illustration of Experiment Setup at IBML.

Because the can is on its side in the experimental configuration, the gamma rays are penetrating through the bottom thickness of the can. To simplify the model and calculation, only the bottom plate of the can, with thickness of 0.33 cm and radius of 1.9 cm, was modeled in CSG and Abaqus/CAE. Volume and surface tallies for photon flux were specified.

Figure 7 shows a comparison of the results from the MCNP6 calculations using CSG and Abaqus/CAE unstructured mesh descriptions. The gamma source is located at -0.64 cm, the surface of the can closest to the beam is at 0.0 cm, and the surface on the inside of the can closest to the sample is at 0.33 cm on the plots. There is about 55% attenuation through the aluminum bottom plate of the can. The drop off in flux that occurs beyond the bottom plate is largely due to the inverse square law and not from attenuation caused by interaction with the air.

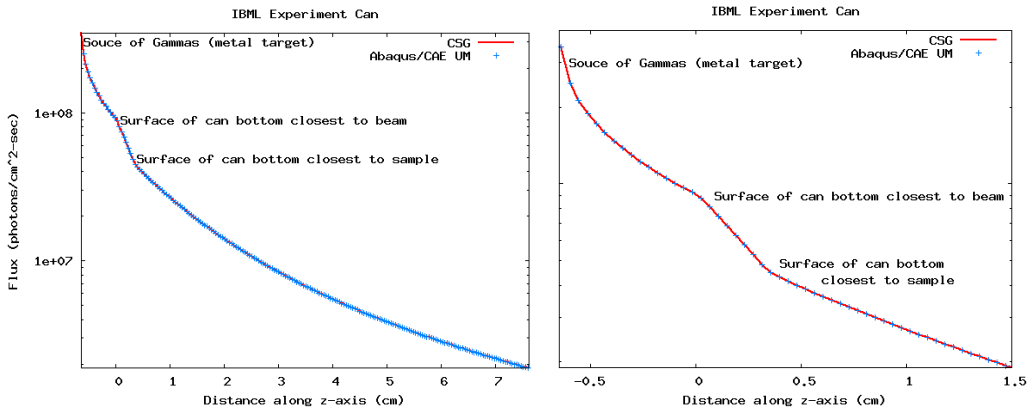

Figure 7. Comparison between MCNP6 photon flux results with CSG and Abaqus/CAE geometry. Plot of flux from source to end of experiment can (left); closer look at photon attenuation through bottom plate of can (right).

The next set of images, Figure 8, compares the visualization of photon flux results calculated by MCNP6 using CSG and unstructured mesh and viewed in the MCNP plotter and Abaqus/CAE.

The images on the left and in the center are from the MCNP plotter and the image on the right is from Abaqus/CAE. It is evident in all of these images that the photon flux is highest in the center of the can bottom which corresponds to the 'beam spot'. The proton beam hits the metal target in a small, circular area; as this occurs, gammas are produced. Although the gammas travel in every direction, more come in contact with the center of the can bottom. Viewing these results with Abaqus/CAE allows the user to remove a section of the can bottom so that the differences in photon flux on the surface as well as through the thickness can be seen simultaneously.

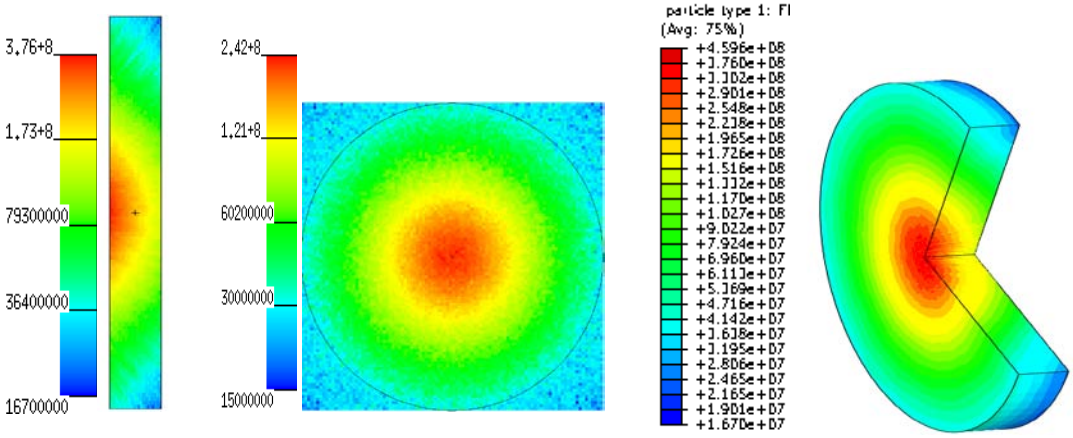

Figure 8. Comparison of photon flux (photons/cm^2-sec).

Results calculated by MCNP6 using CSG and viewed in MCNP's plotter (left and center) and using unstructured mesh and viewed with Abaqus/CAE (right).

3.3 Steel Bar Contaminated with Cobalt-60

The next example problem was inspired by an event that occurred in October 2008, when the French nuclear safety authority was informed that radioactivity was detected in steel elevator buttons at a manufacturing company. After some investigation, it was found that the steel was contaminated with cobalt-60, a radioactive form of the metal (eu-alar.net, 2009). There is some debate over where the contaminated steel came from and exactly how the contamination occurred. Nevertheless, this was not the first time Co-60 contaminated steel was found. It is proposed that because Co-60 sources used for industrial or medical purposes have a metal casing, they can get mixed in with scrap metal and be melted in a steel mill, contaminating the entire batch of steel.

A scenario of a Co-60 contaminated steel bar laying on a concrete mill floor with a lead wall for shielding was modeled. The steel bar is 1 ft. long and has a radius of 2 in. The lead wall is 8 ft. x 8 ft. x 2 in. and 5 ft. away from the steel bar. The concrete floor underneath the steel bar and lead wall is 6 in. thick. A hemisphere of air surrounds the steel bar and wall. An illustration of this scenario is shown in Figure 10. The volume source capability of MCNP6 was tested in this example. This feature works by specifying a 'source' elset in the Abaqus/CAE model.

This elset is pointed to by the ‘volumer’ keyword in the source definition of the MCNP6 input file shown below in Figure 9.

```
sdef  PAR=2  POS=volumer    $ Photon source, position defined by source elset
```

Figure 9. Portion of source definition in MCNP6 input file.

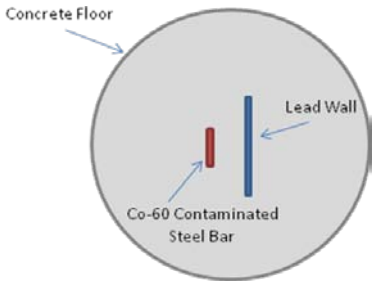

Figure 10. Top planar view of illustration of cobalt-60 contaminated steel bar scenario.

It is desired to obtain results for the dose rate in tissue throughout the room in order to determine where the ‘safe’ areas to stand would be in this situation. Tallies for total photon flux were also added to see the difference in transport through different materials.
The plot in Figure 11 shows a comparison between the MCNP6 calculated photon flux results using CSG and Abaqus/CAE unstructured mesh geometry descriptions. There is near perfect agreement in the area close to the steel bar and lead wall. The differences in the plots in the regions farther away from the source would most likely go away if more histories were run.

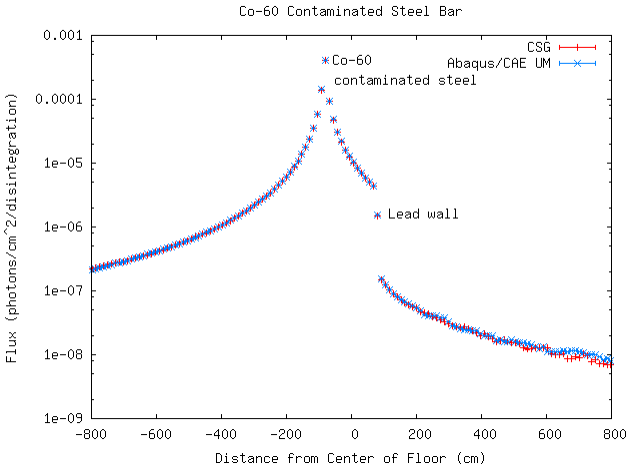

Figure 11. Comparison of MCNP6 photon flux results from using both CSG and Abaqus/CAE geometry descriptions.

Figure 12 shows the visualization of photon flux results throughout the room from the MCNP6 calculations using CSG and unstructured mesh geometries. It can be easily seen that the lead wall

provides shielding from the photons emitted from the Co-60 contaminated steel. It can also be seen in the Abaqus/CAE generated figure that photons can travel farther through air than through the concrete floor.

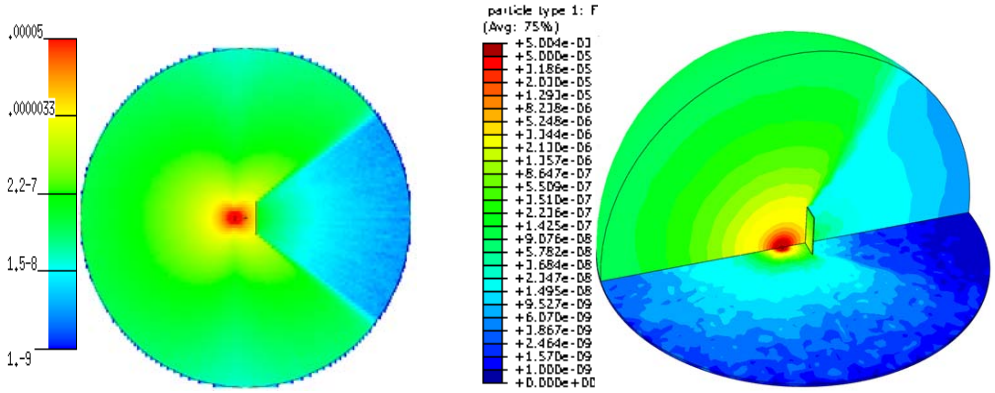

Figure 12. Comparison of photon flux (photons/cm^2-sec) results viewed with MCNP's plotter (left) and Abaqus/CAE (right). Half of the air hemisphere has been removed from the Abaqus/CAE picture for viewing purposes.

Figure 13 shows the individual parts from this scenario (air hemisphere, concrete floor, lead wall, contaminated steel bar). The ability to view results in each part individually is beneficial in problems like this one where looking at the steel bar in the whole picture, it appears that there is no variation in photon flux in the steel; looking at the steel bar on its own reveals that there is variation in flux. There is a higher photon flux in the center of the bar and less towards the outer surface because the steel is providing some shielding of the gammas produced by the cobalt-60.

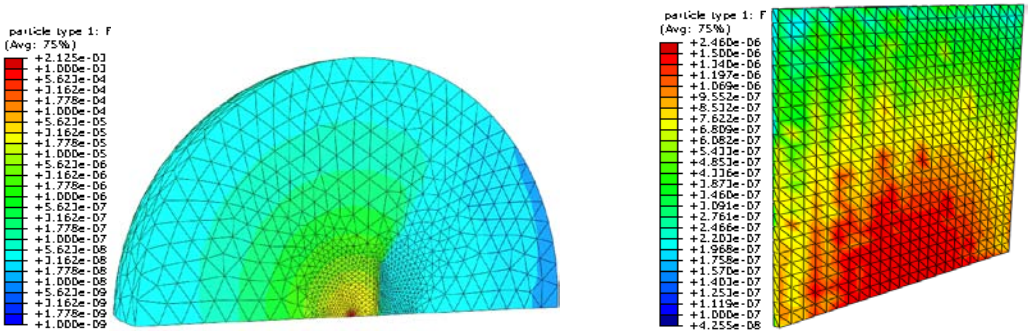

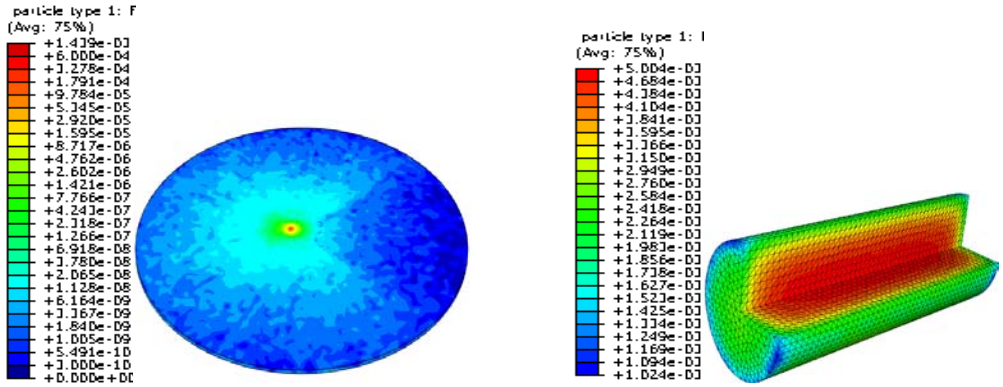

Figure 13. Abaqus/CAE visualization of flux (photons/cm^2-sec) in individual parts from contaminated steel scenario. Air hemisphere (top left), lead wall (top right), concrete floor (bottom left), Co-60 contaminated steel bar (bottom right).

Figure 14 depicts an MCNP mesh tally of the dose rate in tissue throughout the room. The contaminated steel is the yellow region in the center of the picture and the lead wall is on the right side of the picture, clearly shielding photons from that side of the room.

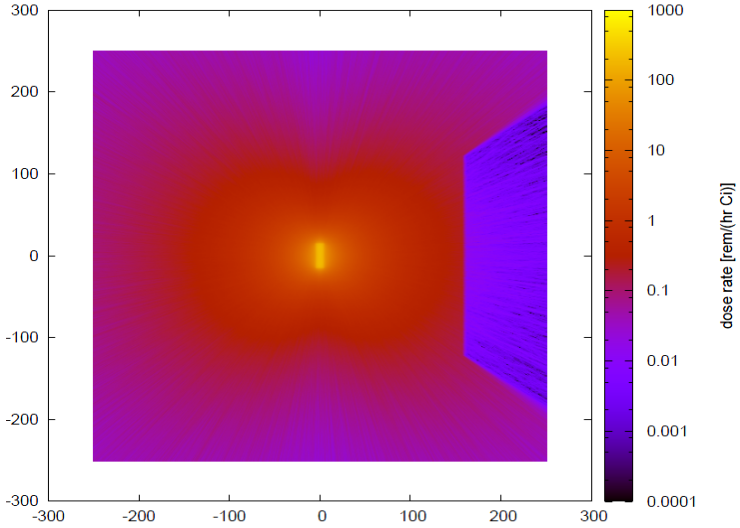

Figure 14. Map of dose rate in room with Co-60 contaminated steel bar and lead wall for shielding.

The following plot, Figure 15, shows dose rates from a 0.4 Ci source along different paths in the room. The path along the x-axis (blue line) goes through the steel bar and then through the lead wall. From left to right in the plot, the dose rate increases up to the steel bar, decreases after the steel, and drops off even more after the lead wall. The path along the y-axis (red line) goes through the steel bar, parallel to the lead wall. The dose rate is nearly constant through the steel bar and decreases with distance from the steel bar. The three horizontal lines show what are

considered very high, high, and radiation areas according to DOE limits. Nowhere in the room is a very high radiation area based on DOE limits. The area within a 1.5 meter perimeter around the steel bar is considered a high radiation area. Outside of that perimeter is a radiation area except for the region that is shielded by the lead wall; that space is not a radiation area.

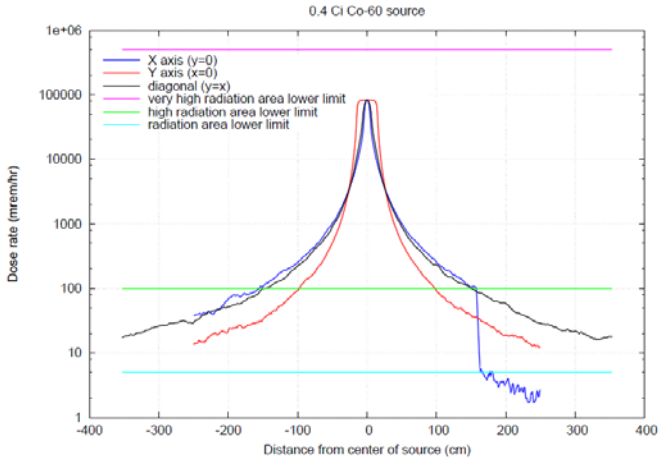

Figure 15. Dose rates along three paths in the room. Also, lines designating areas that are considered very high, high, and radiation areas.

3.4 Experiment Package in ACRR

This example is a simulation of the irradiation of an experiment package in Sandia National Laboratory's (SNL) Annular Core Research Reactor (ACRR). The experiment package is an aluminum can that holds two material sample coupons. The purpose of this problem was to test how an orphan mesh, given by our collaborators at the United Kingdom's Atomic Weapon Establishment (AWE), that was imported into Abaqus/CAE and then embedded into a CSG model of ACRR, would perform. Sandia's published model of ACRR was used (DePriest, 2006). The experiment can was modeled with first order hexahedral elements and a tally for energy deposition in the material sample coupons was specified.

This experiment package was also modeled in CSG and run in MCNP6 using the same model of ACRR. A picture of the set up is shown in Figure 16.

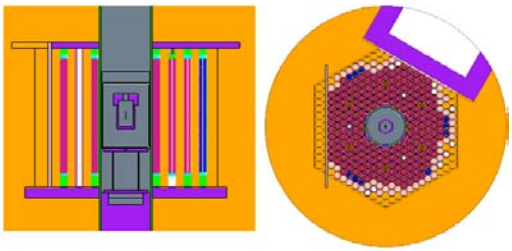

Figure 16. CSG model of ACRR with AWE can. Side planar view (left) shows fuel rod length compared to can. Top planar view (right) shows experiment can surrounded by fuel rods.

Figure 17 shows the results from the MCNP6 run using Abaqus/CAE unstructured mesh geometry. The neutron flux appears even throughout the aluminum can and holder. The coupons in the holder show a more uneven absorption of neutrons. The results are expected to even out if more cycles are run.

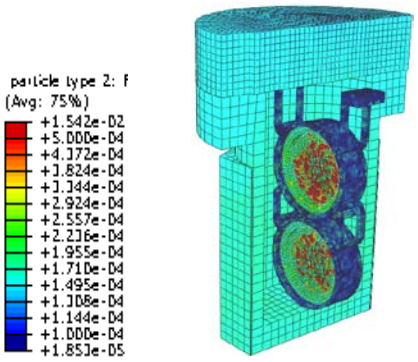

Figure 17. Abaqus/CAE visualization of MCNP6 calculated neutron flux in unstructured mesh model of experiment package in ACRR.

The results for energy deposition in one of the material samples are compared in Table 1. The MCNP6 results from the Abaqus/CAE unstructured mesh run compare very well with the CSG run.

Table 1. Comparison of energy deposition results.

Material	Geometry Description	Energy Deposition	Rel. Error
1	CSG	0.6836	0.0081
1	Abaqus/CAE	0.6836	0.0084

Table 2 displays computer run time comparisons from the models shown in this paper. The same number of histories, 1.00e7, was used for each run. The first three models were run on a 2.76 GHz Intel Xeon Processor. The AWE can was run on a 2.2 GHz Quad-Core AMD Opteron™ Processor. The run time varies according to element type and total number of elements.

Table 2. Computer Runtime Comparisons

Model	Type of elements	Number of Elements	Computer Run Time (min)	Memory (GB)
Lead Wall CSG	N/A	N/A	59.92	0.1
Lead Wall UM	1st Order Hex	9226	229.53	0.1
Steel Bar w/ Co-60 CSG	N/A	N/A	40.01	0.1
Steel Bar w/ Co-60 UM	1st Order Tet	214 402	551.77	0.3
IBML Exp. Can CSG	N/A	N/A	45.94	0.1
IBML Exp. Can UM	1st Order Hex	112 064	224.75	0.3
AWE Exp. Can CSG	N/A	N/A	4289.01	0.2
AWE Exp. Can UM	1st Order Hex	81 586	5449.62	0.4

4. Conclusions

Several example problems that show the use of Abaqus/CAE unstructured mesh as a geometry description for MCNP calculations have been shown in this paper. This way of building geometries has been compared to the legacy CSG and results from calculations using both geometry descriptions have shown to agree well. The benefit to constructing complex geometries and also viewing results with Abaqus/CAE has also been shown. Another benefit to using Abaqus/CAE is that coupling radiation transport with subsequent thermal and mechanical analysis is also possible.

5. Acknowledgements

There are several people who have contributed to this project. Roger Martz is the code developer of MCNP6's hybrid geometry capability. David Crane developed the mesh transport methods and created the script that generates the .odb file for visualization of MCNP6 results in Abaqus/CAE. Our collaborators at AWE created the mesh model of their experiment can. Casey Anderson has done verification and validation of the hybrid geometry capability.

6. References

1. X-5 MONTE CARLO TEAM, "MCNP – A General Monte Carlo N-Particle Transport Code, Version 5, Volume I: Overview and Theory," LA-UR-03-1987, Los Alamos National Laboratory (April 2003).
2. Karen C. Kelley, Roger L. Martz, and David L. Crane, "Riding Bare-Back On Unstructured Meshes For 21st Century Criticality Calculations", PHYSOR 2010 – Advances in Reactor Physics to Power the Nuclear Renaissance, Pittsburgh, Pa, May 9-14, 2010, on CD-ROM, American Nuclear Society, LaGrange Park, IL (2009).
3. Roger L. Martz, private communication, (2011).
4. International handbook of Evaluated Criticality Safety Benchmark Experiments, NEA/NSC/DOC(95) 03 Vol II, (September 2009).
5. "Materials Facility Focus… Ion Beam Materials Laboratory," LALP-06-036.pdf., Los Alamos National Laboratory (2006).
6. The Management of the Co-60 Contamination in Lift Buttons in European Countries, European ALARA Network. http://www.eu-alar.net. (September 2009).
7. K. R. DePriest, P. J. Cooper, and E. J. Parma, "MCNP/MCNPX Model of the Annular Core Research Reactor", Sandia Report SAND2006-3067 (October 2006).